Exploring MHD-Generated Flow in a Triangular Cavity having an elliptic obstruction: Implications for Industrial Applications

Hasan Shahzad[1,2], Abuzar Ghaffari[3 *] , Ghulam Rasool[4,5] , Qiaomei Maa[6], and Yousheng Le[6]

[1]Faculty of Energy and power Engineering, School of Chemical Engineering and Energy Technology, Dongguan University of Technology, China.
[2]Department of Chemical Engineering and Energy Technology, University of Science and Technology. China
[3]Department of Mathematics, Division of Science and Technology, University of Education, Lahore 54770, Pakistan.
[4]Faculty of Materials and Manufacturing, College of Mechanical Engineering and Applied Electronics Technology, Beijing University of Technology, China
[5]Department of mechanical engineering, Lebanese American University, Beirut Lebanon
[6]Faculty of Computer Science, Baoji University of Arts and Sciences, China
Emails**:** hasanshahzad99@hotmail.com, abuzar.ghaffari@ue.edu.pk, grasool@zju.edu.cn , 15489319@qq.com, LYS197902@163.com

Abstract:

Recently, potential applications of double-diffusive (DD) processes have been found in a number of scientific disciplines, including oceanography and geology. With the inclusion of a magnetic field, we numerically analyses the convection energy transfer in a triangular cavity susceptible to solute and diffusion buoyancy effects in this work. For momentum, concentration, and temperature distribution, a Galerkin finite element discretization with quadratic interpolation functions is utilized, and for pressure distribution, we use linear interpolation functions. Elements in the shape of triangles and rectangles are used to discretize the domain. The PARADISO matrix factorized-based nonlinear solver and the Newton method are used to solve nonlinear discretized problems. The analysis of several factors such as Hartmann number $(0-50)$, Rayleigh number (10^4-10^6), Lewis number (0.1-10), and inclination angle $(0°-90°)$ is conducted to investigate the impact of flow on streamlines, isotherms and isoconcentration patterns and graphical and tabular representations are used to show the local heat transfer, kinetic energy, and mass fluxes. Our findings shed light on how DD processes behave in cavities that are exposed to magnetic fields, and they may be useful in optimizing and designing magnetic devices for commercial use.

Keywords: triangular cavity, (MHD) magnetohydrodynamics, finite element method, fillet, numerical simulation

Introduction:

An important dynamical phenomenon, fluid movement inside a cavity has drawn substantial attention in a variety of areas of life. Regarding cavity flow, several scholars worked. Zumbrunnen [1] emphasized the significance of the vortex formulation in the behavior of cavity flow and supported several applications in the synthesis of polymeric composites and drag-reducing riblets.

* abuzar.ghaffari@ue.edu.pk
00923325505532

The researchers have looked at multiple experiments with the impacts of different physical circumstances after reading the literature-cited uses of cavity flow. The two forms of cavity flow are: (1) regular shape cavities and (2) irregular shape cavities. Every cavity form has a unique function in the real world, however recently, a lot of researchers have focused on irregular cavity shapes. In the world of engineering, these cavities are used extensively for cooling electronics, air cooling, collecting solar thermal energy, extracting geothermal energy, and damaging structures. Li et al. [2] using the unique iteration of multiple relaxation time, addressed the flow in a deep cavity. Manca et al. [3] described mixed convection in open cavity bearing heating wall borders into consideration. Aspect ratios of 0.1 to 1.5 and Reynolds numbers between 100 and 1000 were computed, with results. The findings indicated that the temperature decrease is observed for higher Reynolds numbers. They also mentioned aspect ratio performance for various heating configurations in isotherm and streamline patterns. The observed findings further showed the forced flow configuration had maximum level of thermal efficiency at the maximum temperature and heat transfer rate. Khanafer et al. [4] applied in a driven cavity for mixed convection flow, they discovered that depending on how the velocity cycle was conducted, the impacts of Gr and Ra would either accelerate or retard the energy transfer and drag force behavior.

Flack [5] investigated triangular shaped cavities. The statistical properties of right triangular shape cavities were investigated in [6-8]. Polulikakos and Bejan [9] examined the same phenomenon in the bottom-heated right triangular channel numerically and theoretically. Finite element analysis was used by Holtzman et al. [10] to investigate isosceles triangles free of symmetric restrictions. The isosceles triangle was studied symmetrically by Saluman et al. [11]. The natural convection of water in triangles was studied by Lei et al.[12]. In the same Kent. [13] study, heated-bottom isosceles-triangular roofing were analyzed. Same problem discussed by Kent [14] again, this time with top-heated cavities. Research on natural convection flow in a variety of enclosures, including isosceles and right triangles, with a range of boundary conditions was discussed by Wang et al.[15]. Several bottom wall geometries for the triangular hollow were analyzed by Triveni and Panua [16].

Because of its relevance to subjects as diverse as engineering and environmental science, MHD has gained a great deal of interest in recent years. In order to evaluate the effect of magnetic fields on heat transfer, whether through conduction or convection, several research have looked into the impact of MHD on heat transfer in enclosures. In order to investigate the effect of MHD and joule heating on double-diffusive mixed convection in a horizontal channel with an open cavity, Rahman et al. [17] performed a finite element analysis. Teamah [18] studied double diffusive flow in a rectangular cavity subjected to a magnetic field and an internal heat source. They discovered that the fluid circulation, thermal, and diffusive transport rates inside the hollow decreased with increasing magnetic field influence. Kumar et al. [19] describe the results of their study of thermal and diffusive transport in a 2D MHD free convection process taking into account the Soret and Dufour effects. The procedure takes place in a Darcy porous container filled with a thermal and mass fluid that has been stratified. The MHD behaviour of mixed convection heat transfer was investigated in a hexagonal cavity by Ali et al. [20]. The cavity's horizontal walls were held at a steady temperature while the slanted ones were heated. Gireesha et al.[21] studied the natural convection heat transfer of the moving porous radial fin with radiation effects. The governing

equations were solved using shooting technique. The found heat transfer enhanced for the increment of the convective parameter.

In many disciplines of applied science and engineering technology, such as geophysical systems, the phenomenon of natural convection in cavities plays a vital role [22-24], performance of solar energy collectors [25], fire dynamics [26], design of bioreactor [27], fabrication of crystal [28] and the enclosure might have a variety of shapes, including rectangular, circular, elliptical, annular, triangular, or ones with more complicated geometries. Recently, issues with natural convection in the enclosure under various temperature circumstances have caught the attention of researchers. Sarris et al. [29] examined the natural convection in a confined chamber while taking the top wall's sinusoidal temperature into consideration and treating the other walls as insulated. Bahmani and Kargarsharifabad [30-32] conducted a study on natural convection of power-law fluids with laminar flow across a flat plated that is heated horizontally. It was discovered that for $Pr<1$, a decrease in viscosity index leads to increase in wall skin friction, thermal boundary layer thickness, resulting in a lower Nusselt number. The opposite patterns is observed for $Pr>1$. Shahzad et al.[33] investigated the mathematical study of natural convection energy transport in a trapezoidal enclosure caused by the combined buoyancy effects of thermal and solutal diffusion. Umair et al.[34] studied the double diffusive natural convection heat transfer in a waver cavity by a non-Newtonian Casson fluid. They used FEM to discretize and solved the systems of equation. Chamka et al. [35] investigate the entropy generation resulting from the combined effects of MHD mixed convection flow in a gamma shaped enclosure. They found that the presence of nano particles enhance the heat transmission with in the enclosure. Further investigation on natural convection flow can be seen in articles [36-38] and references therein.

An extensive examination of scientific studies highlights a significant lack of study in the investigation of diffusion phenomena when subjected to heat and solutal buoyancy forces. Remarkably, this specific component has received minimal attention, emphasizing the need for additional research and comprehension in this domain. The objective of this study is to examine the fluid dynamics, as well as the characteristics of mass and heat transmission, within a triangular enclosure containing elliptic obstacle. Next section provides a comprehensive explanation of problem formulation and mathematical modeling. Third section provides the solution to the problem, accuracy and effectiveness of the suggested methodology. The study's findings are presented in fourth section though the use of streamlines, isotherms and iso-concentration patterns. Last section provides a concise overview and evaluation of the analysis and finding of the study.

Mathematical Formulation

The physical real problem geometry is shown in Figure 1. Let's consider about the laminar, incompressible, 2-dimension viscous fluid's flow in a certain enclosure. Magnetic field B_0 enforced by an angle γ on horizontal plane. Heat is applied to the cavity's bottom wall at a high concentration (C_h) and constant temperature (T_h). While right and left boundaries are supposed to be cool (T_c) and have less concentration (C_c), respectively. The remainder enclosure is supposed to be adiabatic heated.

Laminar flow, two-dimensional, steady and incompressible are the assumed characteristics. The fluid magneto hydrodynamic motion is appropriate to described using the Navier-Stokes equations.

$$\frac{\partial v}{\partial Y}+\frac{\partial u}{\partial X}=0$$	(1)
$$\mu\left(\frac{\partial^2 u}{\partial x^2}+\frac{\partial^2 u}{\partial y^2}\right)-\frac{\partial p}{\partial x}+F_x=\rho\left(u\frac{\partial u}{\partial x}+v\frac{\partial u}{\partial y}\right)$$	(2)
$$\mu\left(\frac{\partial^2 v}{\partial x^2}+\frac{\partial^2 v}{\partial y^2}\right)-\frac{\partial p}{\partial y}+F_y=\rho\left(u\frac{\partial v}{\partial x}+v\frac{\partial v}{\partial y}\right)$$	(3)
$$\alpha_e\left(\frac{\partial^2 T}{\partial x^2}+\frac{\partial^2 T}{\partial y^2}\right)=u\frac{\partial T}{\partial x}+v\frac{\partial T}{\partial y}$$	(4)
$$D\left(\frac{\partial^2 c}{\partial x^2}+\frac{\partial^2 c}{\partial y^2}\right)=u\frac{\partial c}{\partial x}+v\frac{\partial c}{\partial y}$$	(5)

The problem's relevant boundary conditions

$u=0, v=0, c=c_h, T=T_h$ at Hot side $u=v=0, c=c_c, T=T_c$ at Cold wall $u=v=0, \frac{\partial c}{\partial m}=\frac{\partial T}{\partial m}=0$ at Rest of the side	(6)

Where

$$F_x=\sigma B_0{}^2\left(-u\sin^2\gamma+v\sin\gamma\cos\gamma\right)$$	(7)
$$F_y=\sigma B_0^2\left(-v\cos^2\gamma+u\sin\gamma\cos\gamma\right)+\rho g\left[\beta_c\left(c-c_c\right)+\beta_T\left(T-T_c\right)\right]$$	

For boundary condition *m* represents the normal vector. In order to investigate the influence of relevant parameters, all of these equations are converted into dimensionless form. The following parameters are used to turn equation (1-7) into dimensionless form.

$$(X,Y)=\frac{(x,y)}{L},(U,V)=\frac{(u,v)}{\alpha}L, P=\frac{pL^2}{p\alpha^2},\theta=\frac{c-c_c}{c_h-c_c}, Ra=\frac{\rho^2\beta_\gamma gL^3\Delta T\,\mathrm{Pr}}{v^2},$$ $$Le=\frac{\alpha_e}{D},\alpha_e=\frac{k_e c_h gL^3}{(\rho c_p)_f} Ha=BL\sqrt{\frac{\sigma}{\mu}},\mathrm{Pr}=\frac{v}{\alpha}$$	(8)

By putting equation (8) in equation (1-7), set of ordinary non-linear difference is acquired

$$\frac{\partial V}{\partial Y}+\frac{\partial U}{\partial X}=0$$	(9)
$$\mathrm{Pr}\left(\frac{\partial^2 U}{\partial X^2}+\frac{\partial^2 U}{\partial Y^2}\right)+F_X=\left(U\frac{\partial U}{\partial X}+V\frac{\partial U}{\partial Y}\right)+\frac{\partial p}{\partial X}$$	(10)
$$\mathrm{Pr}\left(\frac{\partial^2 V}{\partial X^2}+\frac{\partial^2 V}{\partial Y^2}\right)+F_Y=\left(U\frac{\partial V}{\partial X}+V\frac{\partial V}{\partial Y}\right)+\frac{\partial p}{\partial X}$$	(11)
$$\left(\frac{\partial^2 \theta}{\partial X^2}+\frac{\partial^2 \theta}{\partial Y^2}\right)=\left(U\frac{\partial \theta}{\partial X}+V\frac{\partial \theta}{\partial Y}\right)$$	(12)
$$\frac{1}{Le}\left(\frac{\partial^2 C}{\partial X^2}+\frac{\partial^2 C}{\partial Y^2}\right)=\left(U\frac{\partial C}{\partial X}+V\frac{\partial C}{\partial Y}\right)$$	(13)

The boundary values condition's dimensionless form

$U=0, V=0, C=1, \theta=1$ at Hot side $U=V=0, C=0, \theta=0$ at cold side $U=0, V=0, \frac{\partial c}{\partial m}=\frac{\partial T}{\partial m}=0$ at Rest of the side	(14)

Where

$$F_X=\mathrm{Pr}\,Ha^2\left(-U\sin^2\gamma+v\sin\gamma\cos\gamma\right)$$	(15)
$$F_Y=\mathrm{Pr}\,Ha^2\left(-V\cos^2\gamma+U\sin\gamma\cos\gamma\right)+\mathrm{Pr}\,Ra(Nc+\theta)$$	

The Nusselt number *(Nu)*, average Nusselt number (Nu_{avg}), Sherwood number(Sh), average Sherwood number(Sh_{avg}) and kinetic energy$(K.E)$ on the hot side in triangular cavity can be defined as

$$Nu = \left(-\frac{\partial \theta^*}{\partial X^*} \right)_{X^*=0}$$	(16)
$$Nu_{avg} = \int_0^1 Nu \, dY$$	(7)
$$Sh = \left(-\frac{\partial C^*}{\partial X^*} \right)_{X^*=0}$$	(18)
$$Sh_{avg} = \int_0^1 sh \, dY$$	(19)
$$K.E = \frac{1}{2} \int_\Omega \|U\|^2 \, d\Omega$$	(20)

Solution Methodology

The equations (9-14) are highly nonlinear and cannot be solved analytically. In order to tackle the nonlinear discrete system of equations, the Newton method is used in conjunction with a direct solver called PARDISO. PARDISO utilizes the LU factorization, which helps to minimize the amount of cycles needed to achieve the desired level of convergence. The iterative process for dealing with non-linearity ceased after certain threshold factor is verified. The detail methodology is explained in the articles [34, 39-41] and references therein.

Weak formulation:

The given expression represents the weak form of equations (9)-(14)

$$\int_A \left(\frac{\partial U}{\partial X} + \frac{\partial V}{\partial Y} \right) w \, dA = 0$$	(21)
$$\int_A \left(U \frac{\partial U}{\partial X} + V \frac{\partial U}{\partial Y} \right) w \, dA + \int_A \frac{\partial P}{\partial X} w \, dA - \Pr \int_A \left(\frac{\partial^2 U}{\partial X^2} + \frac{\partial^2 U}{\partial Y^2} \right) w \, dA - \int_A \xi_X w \, dA = 0$$	(22)

$$\int_A \left(U \frac{\partial V}{\partial X} + V \frac{\partial V}{\partial Y} \right) w \, dA + \int_A \frac{\partial P}{\partial Y} w \, dA - \Pr \int_A \left(\frac{\partial^2 V}{\partial X^2} + \frac{\partial^2 V}{\partial Y^2} \right) w \, dA - \int_A \xi_\gamma w \, dA = 0$$	(23)
$$\int_A \left(U_k \frac{\partial \theta_k}{\partial X} + V_k \frac{\partial \theta_{\partial k}}{\partial Y} \right) w_k \, dA - \int_A \left(\frac{\partial^2 \theta_k}{\partial X^2} + \frac{\partial^2 \theta_k}{\partial Y^2} \right) w_k \, dA = 0$$	(24)
$$\int_A \left(U_k \frac{\partial C_k}{\partial X} + V_k \frac{\partial C_k}{\partial Y} \right) w_k \, dA - \frac{1}{L_e} \int_A \left(\frac{\partial^2 C_k}{\partial X^2} + \frac{\partial^2 C_k}{\partial Y^2} \right) w_k \, dA = 0$$	(25)

In order to obtain a numerical approximation, we compare the solutions obtained from continuous and discrete methods within finite dimensional sub-spaces

$$U \approx U_k \quad V \approx V_k \quad \theta \approx \theta_k \quad \in \quad w_k \begin{Bmatrix} C \approx C_k \in q_k \\ P \approx P_k \in Q_k \end{Bmatrix}$$	(26)

Using equation 28 into above equation the discrete version is as follow

$$\int_A \left(\frac{\partial U_k}{\partial X} + \frac{\partial V_k}{\partial Y} \right) w_k \, dA = 0$$	(27)
$$\int_A \left(U_k \frac{\partial U_k}{\partial X} + V_k \frac{\partial U_k}{\partial Y} \right) w_k \, dA + \int_A \frac{\partial P_k}{\partial X} w_k \, dA - \Pr \int_A \left(\frac{\partial^2 U_k}{\partial X^2} + \frac{\partial^2 U_k}{\partial Y^2} \right) w_k \, dA - \int_A \xi_X w_k \, dA = 0$$	(28)
$$\int_A \left(U_k \frac{\partial \theta_k}{\partial X} + V_k \frac{\partial \theta_{\partial k}}{\partial Y} \right) w_k \, dA - \int_A \left(\frac{\partial^2 \theta_k}{\partial X^2} + \frac{\partial^2 \theta_k}{\partial Y^2} \right) w_k \, dA = 0$$	(29)
$$\int_A \left(U_k \frac{\partial C_k}{\partial X} + V_k \frac{\partial C_k}{\partial Y} \right) w_k \, dA - \frac{1}{L_e} \int_A \left(\frac{\partial^2 C_k}{\partial X^2} + \frac{\partial^2 C_k}{\partial Y^2} \right) w_k \, dA = 0$$	(30)

For discrete solution the basic function is as follow

$$\left.\begin{aligned} U_k &\approx \sum_{h=1}^{N} U_h \phi_h(x,y) \qquad \theta_k \approx \sum_{h=1}^{N} \theta_h \theta_h(x,y) \\ V_k &\approx \sum_{h=1}^{N} V_h \phi_h(x,y) \qquad C_k \approx \sum_{h=1}^{N} C_h C_h(x,y) \\ P_k &\approx \sum_{h=1}^{N} P_h \Psi_h(x,y) \end{aligned}\right\}$$	(31)
$$\int_A \left(\frac{\partial U_k}{\partial X} + \frac{\partial V_k}{\partial Y} \right) w_k \, dA = 0$$	(32)
$$\int_A \left(U_k \frac{\partial V_k}{\partial X} + V_k \frac{\partial V_k}{\partial Y} \right) w_k \, dA + \int_A \frac{\partial P_k}{\partial y} w_k \, dA - \Pr \int_A \left(\frac{\partial V_k}{\partial X} \frac{\partial w_k}{\partial X} + \frac{\partial V_k}{\partial Y} \frac{\partial w_k}{\partial Y} \right) w_k \, dA - \int_A \xi_X w_k \, dA = 0$$	(33)
$$\int_A \left(U_k \frac{\partial V_k}{\partial X} + V_k \frac{\partial V_k}{\partial Y} \right) w_k \, dA + \int_A \frac{\partial P_k}{\partial y} w_k \, dA - \Pr \int_A \left(\frac{\partial V_k}{\partial X} \frac{\partial w_k}{\partial X} + \frac{\partial V_k}{\partial Y} \frac{\partial w_k}{\partial Y} \right) w_k \, dA - \int_A \xi_X w_k \, dA = 0$$	(34)
$$\int_A \left(U_k \frac{\partial \theta_k}{\partial X} + V_k \frac{\partial \theta_{\partial k}}{\partial Y} \right) w_k \, dA - \int_A \left(\frac{\partial \theta_k}{\partial X} \frac{\partial w_k}{\partial X} + \frac{\partial \theta_k}{\partial Y} \frac{\partial w_k}{\partial Y} \right) w_k \, dA = 0$$	(35)
$$\int_A \left(U_k \frac{\partial C_k}{\partial X} + V_k \frac{\partial C_k}{\partial Y} \right) w_k \, dA - \frac{1}{L_e} \int_A \left(\frac{\partial C_k}{\partial X} \frac{\partial w_k}{\partial X} + \frac{\partial C_k}{\partial Y} \frac{\partial w_k}{\partial Y} \right) w_k \, dA = 0$$	(36)

The parameters retain their typical definitions, and in order to obtain the solution, the non-linear system is iteratively processed until a certain threshold of tolerance is reached.

Grid convergence

Several grids were used for $Le = 1$, $Ra = 10^5$, $Ha = 15$ and $Pr = 6.8$ to demonstrate the result's efficacy (table 1). Both the total number of elements (#EL) and the number of degrees of freedom (DOFs) ranged anywhere from 396 to 20908 correspondingly and from 4662 all the way up to 193600 respectively. Following an examination of the average Nusselt number, for the two grids (L8 and L9), it was discovered that there was hardly any variation between them. As a result, there was grid independence supplied by 157798 DOF and 16696 #EL, and the results that were reported

are based on these values. Figure 1b depicts the largest mesh size that was used for this investigation. For this study, the coarsest mesh size is shown in Fig.1b.

Code validation

After grid independence is achieved, we reproduced existing results of Oztop and Abu-Nada [41]. Fig. 2 shows the agreement between the two isotherms, demonstrating that our data is reliable and can be trusted.

Discussion and Result

Being compared to a wide variety of pertinent physical factors, such as the Rayleigh number (Ra), Hartmann number (Ha), and Lewis number (Le), the interpretation of the data is displayed in the form of concentration distribution, streamlines and isotherms. The mass flux coefficient, heat flux coefficient, and K.E are additional global and local parameters that are determined.

Impacts of Ha

Table 2 illustrates how Ha affects, the heat and mass transfer rate $\left(for\ Ra = 10^4, 10^5, and\ 10^6 \right)$ respectively. Heat and mass transfer rate reduces for increasing values of Hartmann number which indicate the reduction in velocity of the system. The impact of Rayleigh number on heat and mass transfer rate is opposite to that of Hartman number hence increasing hence increase Ra increases the velocity inside the enclosure. The effects of Ha on streamline, isothermal, and iso-concentration contours are shown in Fig. 3. It clearly shows that the intensity of streamline circulation decreases as Ha values increase. Furthermore, it is evident that the thickness of the thermal boundary layer reduces as Ha increases. On the other hand, at lower boundary wall, circulation strength rises with rising Ha, and the thermal boundary layer is thicker.

Impact of Rayleigh number

Table 2 illustrates how Rayleigh number (Ra) affects, the heat and mass transfer rate $(\gamma = 0^o,\ \gamma = 30^o,\ and\ \gamma = 60^o)$ respectively. Heat and mass transfer rate increases for increasing values of Ra. Higher Ra values result in smoother isothermal and isoconcentration contours and a sharper streamline at the triangle's slope, as seen in Fig. 4. The inverse effect is observed for isothermal and isoconcentration contours. Also, heat and mass transfer rate has maximum value at $\gamma = 30^o$ and its values reduces for $\gamma = 0^o$ and $\gamma = 60^o$ (see Table 3.).

Impact of Lewis number

Table 4 illustrates how Lewis number (Le) affects, the heat and mass transfer rate (for $Ra = 10^4, 10^5,$ and 10^6) respectively. Lewis number has different impact on heat transfer rate. Heat transfer rate for $Ra = 10^4$ increases from $0.1 \le Le \le 7.5$ then decreases. Nusselt number for $Ra = 10^5$ increases from $0.1 \le Le \le 5$ then decreases. For large values of Rayleigh number $Ra = 10^6$, heat transfer rate decreases for variation in Le. Sherwood number has dominated effect on mass transfer rate. Mass transfer rate increases for increasing values of Le. Fig. 5 describe the iso-concentration, isotherms, and streamlines for varying Le. As Le increases, the streamlines become more strongly circulated. The isoconcentration and isothermal contours are forced towards wall's lower side, while in lower section of the tri-angular cavity their contours show more concentration.

A 3D view of concentration for variation in Lewis number is shown in Fig. 6. The figure clearly shows that for $Le = 0.1$, the concentration is highest at the bottom; as Le grows, the concentration inside the enclosure rises correspondingly.

Fig.7 shows the impact of Hartmann number on velocity, concentration and temperature. Due to the Lorentz force's there is increase in resistance that decreased the velocity. While, heat and concentration increases with increasing values of Ha.

Fig. 8 shows effect by Le on velocity, concentration and temperature. As Le increases, velocity and concentration decrease, while temperature remains relatively unchanged.

The impact of Rayleigh number (Ra) on concentration, temperature and velocity. profiles are depicted in Fig. 9. The is increase in velocity for increasing values of Ra, but the temperature profile and the right and left side's concentration profile exhibit random disruption on the bottom wall.

The heat (a) and mass (b) transfer rate versus Hartmann number for variation in Ra for $(\gamma = 30^{\circ}, N = 1, \Pr = 6.8)$ is plotted in Fig. (10). The heat and mass transfer has maximum values for pure hydrodynamic case $(Ha = 0)$. When the value of Hartmann number increases the heat and mass transfer rate starts decreasing.

Table 5 shows the average kinetic energy changing for variation in Hartmann number, magnetic field inclination angle and Lewis number. K.E decreases for increasing values of Ha and have

increasing trend for Le. At $Ra = 10^6$, and $Ha = 0$, the K.E is enhanced by a factor of 2257 compared to $Ra = 10^4$ and $Ha = 0$.

Conclusion

In the current communication, a triangular enclosure with uniform concentration and thermal distributions is studied for viscous flow by Double Diffusive Natural Convection. To prevent singularity development in the computational domain, fillets are employed at the cavity's corners. Governing equations for the problem are formulated in dimensionless form and solved by applying finite element procedures. The resulting momentum, temperature, and concentrate distributions, as well as the isothermal and iso-concentration patterns, all exhibit modifications as a result of the numerical simulation. Also, as a function of the relevant physical parameters, variables of engineering importance including local heat, kinetic energy, and mass flow coefficients are calculated. The key findings are summarized as.

- Velocity is maximum for pure hydrodynamic case $(Ha = 0)$, but for variation in Hartmann number it decreases. Hence, concentration and temperature profiles decreases.
- For $Ra = 10^4$ streamlines patterns shows the flow is dominant near bottom wall but for the variation in Rayleigh number streamlines are equally distributed in the whole enclosure around the elliptic obstacle, which clearly indicates the increase in velocity. Rayleigh number enhances the heat and mass transfer rate significantly.
- There is no noticeable alteration in streamlines and isotherms for the variation in Lewis number since it is not directly related to momentum diffusivity. However, fluid concentration rises with in enclosure for variation in Le.
- γ and Le significantly affect the Sherwood profiles and Nusselt number.

In future research, the model being explored might be expanded to investigate entropy generation, micropolar fluids, nano and hybridnano fluids in various configurations.

Author Contribution:

All authors contributed equally in the article in conceptualization, investigation, analysis, writing original draft, review and editing.

Nomenclature

x & y	*x and y coordinate (m)*	X & Y	*X and Y coordinate*
p	*Fluid Pressure (Pa)*	P	*Fluid Pressure*
c	*Concentration* $(Kg.m^{-3})$	C	*Concentration*
T	*Temperature (K)*	θ	*Temperature*
u&v	*Velocity components along x &y*	U&V	*Velocity components along X&Y*
Symbols			
γ	*Angle (Inclination) (rad)*	Le	*Lewis number*
ρ	*Fluid density* $(kg.m^{-3})$	N	*Buoyancy ratio*
g	*Gravity (m/s)*	Ra	*Rayleigh number*
B	*Magnetic Field (Tesla)*	Pr	*Prandtl number*
B_0	*Magnetic field strength (Tesla)*	Sh_{avg}	*Averaged Sherwood number*
c_p	*Specific Heat* $(J.Kg^{-1}.K^{-1})$	Sh	*Sherwood number (local)*
K.E	*Total Kinetic energy (J)*	DOF	*Degree of freedom*
T_h&c_h	*High temperature & concentration*	$\#EL$	*Number of elements*
T_c&c_c	*Low temperature and concentration*	Nu	*Nusselt number (local)*
ρ	*Fluid density*	Nu_{avg}	*Averaged Nusselt number*
μ	*Kinematic viscosity*	Ha	*Hartmann number*
g	*gravity*		

References

1. **Zumbrunnen, D., Miles, K., and Liu, Y.** "Auto-processing of very fine-scale composite materials by chaotic mixing of melts." *Composites Part A: Applied Science and Manufacturing*, vol. 27, no. 1, 1996, pp. 37-47. doi:10.1016/1359-835X(95)00045-D
2. **Lin, L.-S., Chen, Y.-C., and Lin, C.-A.** "Multi relaxation time lattice Boltzmann simulations of deep lid driven cavity flows at different aspect ratios." *Computers & Fluids*, vol. 45, no. 1, 2011, pp. 233-240. doi:10.1016/j.compfluid.2010.12.017
3. **Manca, O., Nardini, S., and Ricci, D.** "Effect of heated wall position on mixed convection in a channel with an open cavity." *Numerical Heat Transfer: Part A: Applications*, vol. 43, no. 3, 2003, pp. 259-282. doi:10.1080/10407780390173843
4. **Khanafer, K., Vafai, K., and Lightstone, M.** "Buoyancy-driven heat transfer enhancement in a two-dimensional enclosure utilizing nanofluids." *International Journal of Heat and Mass Transfer*, vol. 46, no. 19, 2003, pp. 3639-3653. doi:10.1016/S0017-9310(03)00156-X.
5. **Flack Jr, R. and C. Witt**, Velocity measurements in two natural convection air flows using a laser velocimeter *AMSE Journal of Heat and Mass Transfer* vol. 46, no. 101, 1979, pp. 256-260 doi: doi.org/10.1115/1.3450956
6. **Flack, R., T. Konopnicki, and J. Rooke,** *The measurement of natural convective heat transfer in triangular enclosures. AMSE Journal of Heat and Mass Transfer* vol. 46, no. 101, 1979, pp. 648-654. doi: doi.org/10.1115/1.3451051
7. **Akinsete, V.A., and Coleman, T.** "Heat transfer by steady laminar free convection in triangular enclosures." *International Journal of Heat and Mass Transfer*, vol. 25, no. 7, 1982, pp. 991-998. doi:10.1016/0017-9310(82)90004-4.

8. **Flack, R. D.** "The experimental measurement of natural convection heat transfer in triangular enclosures heated or cooled from below." *ASME Journal of Heat and Mass Transfer*, vol. 102, 1980, pp. 770-772. doi:10.1115/1.3244389.
9. **Poulikakos, D., and Bejan, A.** "The fluid dynamics of an attic space." *Journal of Fluid Mechanics*, vol. 131, 1983, pp. 251-269. doi:10.1017/S0022112083000145.
10. **Holtzman, G., Hill, R., and Ball, K.** "Laminar natural convection in isosceles triangular enclosures heated from below and symmetrically cooled from above." *Journal of Heat Transfer*, vol. 122, no. 3, 2000, pp. 485-491. doi:10.1115/1.1283791.
11. **Salmun, H.** "The stability of a single-cell steady-state solution in a triangular enclosure." *International Journal of Heat and Mass Transfer*, vol. 38, no. 2, 1995, pp. 363-369. doi:10.1016/0017-9310(94)00133-H.
12. **Lei, C., Armfield, S.W., and Patterson, J.C.** "Unsteady natural convection in a water-filled isosceles triangular enclosure heated from below." *International Journal of Heat and Mass Transfer*, vol. 51, no. 11-12, 2008, pp. 2637-2650. doi:10.1016/j.ijheatmasstransfer.2007.11.002.
13. **Kent, E.F.** "Laminar natural convection in isosceles triangular roofs in wintertime conditions." *Heat Transfer Engineering*, vol. 31, no. 13, 2010, pp. 1068-1081. doi:10.1080/01457632.2010.501222.
14. **Kent, E.F.** "Numerical analysis of laminar natural convection in isosceles triangular enclosures for cold base and hot inclined walls." *Mechanics Research Communications*, vol. 36, no. 4, 2009, pp. 497-508. doi:10.1016/j.mechrescom.2009.06.005
15. **Wang, Q., Zhang, Y., and Xu, J.** "Numerical analysis on natural convection in various enclosures." *Numerical Heat Transfer, Part A: Applications*, vol. 77, no. 4, 2020, pp. 391-408. doi:10.1080/10407782.2020.1728581
16. **Triveni, M.K., and Panua, R.** "Numerical analysis of natural convection in a triangular cavity with different configurations of hot wall." *International Journal of Heat and Technology*, vol. 35, no. 1, 2017, pp. 11-18. doi:10.18280/ijht.350102
17. **Rahman, M., Saidur, R., and Rahim, N.** "Conjugated effect of joule heating and magneto-hydrodynamic on double-diffusive mixed convection in a horizontal channel with an open cavity." *International Journal of Heat and Mass Transfer*, vol. 54, no. 15-16, 2011, pp. 3201-3213. doi:10.1016/j.ijheatmasstransfer.2011.03.022
18. **Teamah, M.A.** "Numerical simulation of double diffusive natural convection in rectangular enclosure in the presence of magnetic field and heat source." *International Journal of Thermal Sciences*, vol. 47, no. 3, 2008, pp. 237-248. doi:10.1016/j.ijthermalsci.2007.05.008
19. **Kumar, V., Murthy, S.K., and Kumar, B.R.** "Influence of MHD forces on Bejan's heatlines and masslines in a doubly stratified fluid saturated Darcy porous enclosure in the presence of Soret and Dufour effects – A numerical study." *International Journal of Heat and Mass Transfer*, vol. 117, 2018, pp. 1041-1062. doi:10.1016/j.ijheatmasstransfer.2017.09.062
20. **Ali, M.M., Alim, M., and Ahmed, S.S.** "Magnetohydrodynamic mixed convection flow in a hexagonal enclosure." *Procedia Engineering*, vol. 194, 2017, pp. 479-486. doi:10.1016/j.proeng.2017.08.169.
21. **Mahanthesh, B., and Gireesha, B.** "Thermal Marangoni convection in two-phase flow of dusty Casson fluid." *Results in Physics*, vol. 8, 2018, pp. 537-544. doi:10.1016/j.rinp.2018.03.008

22. **Llanos, E.M., Zarrouk, S.J., and Hogarth, R.A.** "Numerical model of the Habanero geothermal reservoir, Australia." *Geothermics*, vol. 53, 2015, pp. 308-319. doi:10.1016/j.geothermics.2015.05.002
23. **Shoeibi, S., Shokouhian, A., and Karami, H.** "Application of simultaneous thermoelectric cooling and heating to improve the performance of a solar still: an experimental study and exergy analysis." *Applied Energy*, vol. 263, 2020, p. 114581. doi:10.1016/j.apenergy.2020.114581
24. **Shoeibi, S., Shokouhian, A., and Karami, H.** "Energy matrices, exergoeconomic and enviroeconomic analysis of air-cooled and water-cooled solar still: Experimental investigation and numerical simulation." *Renewable Energy*, vol. 171, 2021, pp. 227-244. doi:10.1016/j.renene.2021.03.061.
25. **Bég, O.A., Bég, S.A., and Alkhateeb, A.** "Computational modeling of heat transfer in an annular porous medium solar energy absorber with the P1-radiative differential approximation." *Journal of the Taiwan Institute of Chemical Engineers*, vol. 66, 2016, pp. 258-268. doi:10.1016/j.jtice.2016.05.022
26. **Hasemi, Y., and Tokunaga, T.** "Some experimental aspects of turbulent diffusion flames and buoyant plumes from fire sources against a wall and in a corner of walls." *Combustion Science and Technology*, vol. 40, no. 1-4, 1984, pp. 1-18. doi:10.1080/00102208408951127
27. **Bhargava, R., Singh, M., and Jha, A.** "Finite element simulation of nonlinear convective heat and mass transfer in a micropolar fluid-filled enclosure with Rayleigh number effects." *International Journal of Applied and Computational Mathematics*, vol. 3, 2017, pp. 1347-1379. doi:10.1007/s40819-017-0371-4
28. **Gelfgat, A.Y.** "On three-dimensional instability of a traveling magnetic field driven flow in a cylindrical container." *Journal of Crystal Growth*, vol. 279, no. 3-4, 2005, pp. 276-288. doi:10.1016/j.jcrysgro.2005.03.012
29. **Yücel, A., Acharya, S., and Williams, M.** "Natural convection and radiation in a square enclosure." *Numerical Heat Transfer*, vol. 15, no. 2, 1989, pp. 261-278. doi:10.1080/10407788908913931
30. **Bahmani, A., and Kargarsharifabad, H.** "Laminar natural convection of power-law fluids over a horizontal heated flat plate." *Heat Transfer—Asian Research*, vol. 48, no. 3, 2019, pp. 1044-1066. doi:10.1002/htj.22481
31. **Bahmani, A., and Kargarsharifabad, H.** "Magnetohydrodynamic free convection of non-Newtonian power-law fluids over a uniformly heated horizontal plate." *Thermal Science*, vol. 24, no. 2 Part B, 2020, pp. 1323-1334. doi:10.2298/TSCI190626176B
32. **Bahmani, A., and Kargarsharifabad, H.** "New integral solutions for magnetohydrodynamic free convection of power-law fluids over a horizontal plate." *Iranian Journal of Science and Technology, Transactions of Mechanical Engineering*, vol. 45, 2021, pp. 1091-1101. doi:10.1007/s40940-021-00283-0
33. **Shahzad, H., Khan, I., and Ahmad, F.** "Double-diffusive natural convection energy transfer in magnetically influenced Casson fluid flow in trapezoidal enclosure with fillets." *International Communications in Heat and Mass Transfer*, vol. 137, 2022, p. 106236. doi:10.1016/j.icheatmasstransfer.2022.106236
34. **Rashid, U., Shahzad, H., and Khan, I.** "Non-Newtonian MHD double diffusive natural convection flow and heat transfer in a crown enclosure." *Case Studies in Thermal Engineering*, vol. 41, 2023, p. 102541. doi:10.1016/j.csite.2023.102541

35. **Chamkha, A.J., Abidi, M., and Alharbi, M.** "Magnetohydrodynamic mixed convection and entropy analysis of nanofluid in gamma-shaped porous cavity." *Journal of Thermophysics and Heat Transfer*, vol. 34, no. 4, 2020, pp. 836-847. doi:10.2514/1.T5811
36. **Chamkha, A.J., Abidi, M., and Alharbi, M.** "MHD convection of an Al2O3–Cu/water hybrid nanofluid in an inclined porous cavity with internal heat generation/absorption." *Iranian Journal of Chemistry and Chemical Engineering*, vol. 41, no. 3, 2022, pp. 936-956. doi:10.30492/IJCCE.2022.247148.1644
37. **Kargarsharifabad, H.** "Optimization of arrangement of conducting fins and insulated obstacles inside a cavity: the couple of numerical solutions and genetic algorithm methods." *Journal of Thermal Analysis and Calorimetry*, vol. 147, no. 1, 2022, pp. 421-433. doi:10.1007/s10973-021-10490-2
38. **Falsafi, M., et al.** "Numerical investigation of forced convective heat transfer of ferrofluid in a pipe under a magnetic field." *Numerical Methods in Engineering*, vol. 34, no. 1, 2022, pp. 11-25. doi:10.1016/j.numere.2022.01.001
39. **Aslam, M.A., Shahzad, H., and Khan, I.** "Numerical analysis of double-diffusive natural convective flow of Ostwald-de Waele fluid in an irregular enclosure with a circular obstacle." *Results in Physics*, 2023, p. 107312. doi:10.1016/j.rinp.2023.107312
40. **Aslam, M.A., Shahzad, H., and Khan, I.** "Finite element modeling of dual convection in a Y-shaped porous cavity containing viscous fluid." *Frontiers in Physics*, vol. 11, 2023, pp. 1-13. doi:10.3389/fphy.2023.107312
41. **Chuhan, I.S., Shahzad, H., and Khan, I.** "Entropy optimization of MHD non-Newtonian fluid in a wavy enclosure with double diffusive natural convection." *Numerical Heat Transfer, Part A: Applications*, 2023, pp. 1-21. doi:10.1080/10407782.2023.2245621

Biographies

Hasan Shahzad:

Dr. Hasan Shahzad is a passionate researcher and academic with expertise in fluid mechanics, heat transfer, and computational modeling. Currently a postdoctoral researcher at Dongguan University of Technology, his work focuses on mathematical modeling and numerical simulations for energy systems and thermal management in advanced technologies. With a PhD in Applied Fluid Mechanics from Beijing University of Technology and a Master's degree in Applied Mathematics, Dr. Shahzad has contributed extensively to areas like nanofluids, MHD flows, and proton exchange membrane fuel cells (PEMFCs). He is also an active reviewer and editor for leading international journals, demonstrating a commitment to advancing research and academic excellence.

Dr. Abuzar Ghaffari is a distinguished Assistant Professor of Mathematics at the University of Education, Lahore, Attock Campus. He earned his Ph.D. in Mathematics from the International Islamic University, Islamabad, where he developed expertise in advanced mathematical and computational techniques. Dr. Ghaffari has a research interest in modeling, simulation and statistical computing. He has made significant contributions to the study of boundary layer flows, stability analysis, and sensitivity analysis, offering valuable insights into complex mathematical phenomena.

Ghulam Rasool:

Dr. Ghulam Rasool is a Pakistani national currently serving as an Assistant Professor in the Department of Mathematics at PMU, KSA holding a Ph.D. from Zhejiang University, China. With several years of teaching and research experience, Dr. Rasool has made significant contributions in theory and implementation techniques of fluid flow models to optimize heat transfer management using various linear and nonlinear stretching surfaces, Latent Heat & Thermal Energy Storage (LHTES), Thermal Energy Storage (TES), and battery management systems. Dr. Rasool's research interests encompass heat transfer enhancement mechanisms, latent heat & energy storage, computational fluid dynamics, and the optimization of forced convection heat transfer systems, with a focus on entropy optimization concerning nanofluids.

Qiaomei Maa and Yousheng Le: are PhD candidate at Baoji University of Arts and Sciences.

Figure 1: Schematic diagram of the problem.

(A) (B)

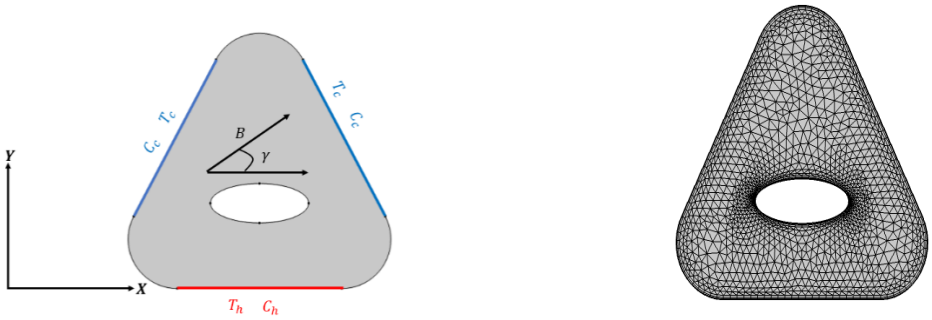

Figure 2: (a) present (b) H.F. Oztop, E. Abu-Nada [41] (Isotherms)

(a) (b)

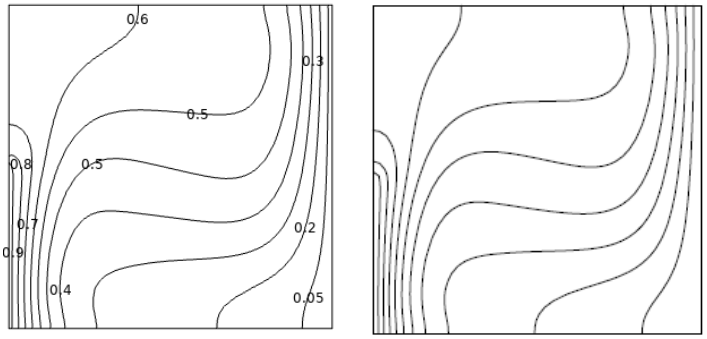

Table 1 - Grid independency test

Grid	#El	DOF	Nu_{ava}
L1	396	4662	3.1803
L2	567	6498	3.2208
L3	837	9252	3.2456
L4	1405	14998	3.3016
L5	1815	18993	3.3377
L6	2786	28088	3.3523
L7	6321	62139	3.4220
L8	16696	157798	3.4612
L9	20908	193600	3.4612

Figure 3. ($\gamma = 0,\ Ra = 10^5,\ Le = 2.5$)

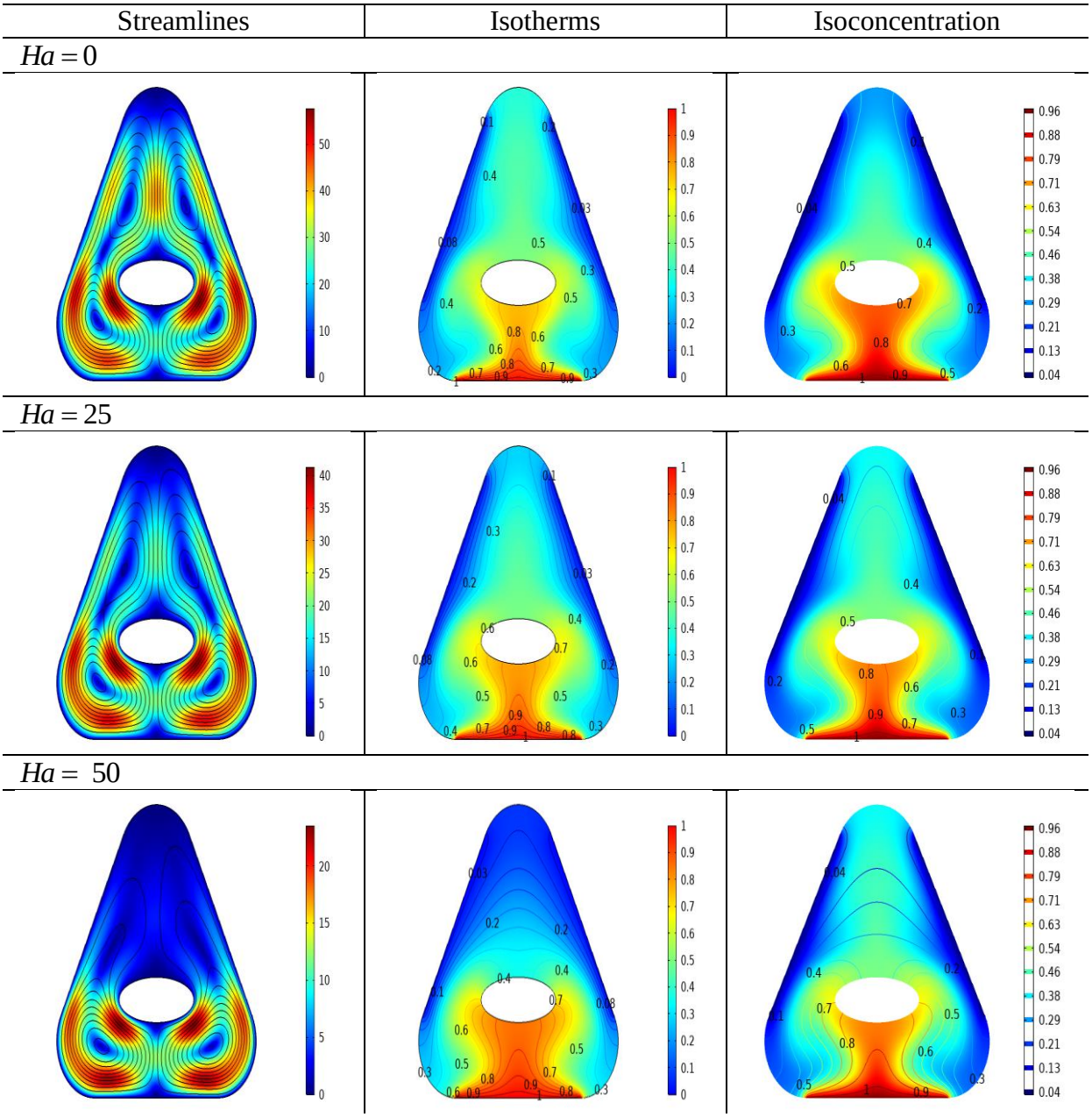

Figure 4: ($\gamma = 0,\ Le = 2.5,\ Ha = 20$)

Streamlines	Isotherms	Isoconcentration
$Ra = 10^4$		
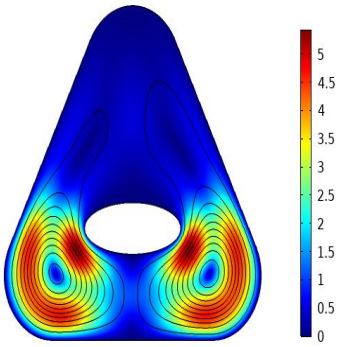	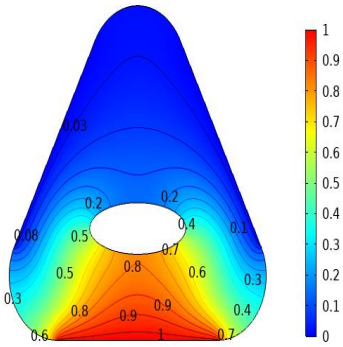	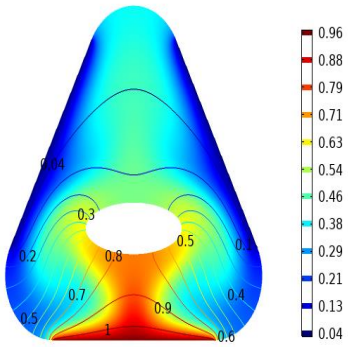
$Ra = 10^5$		
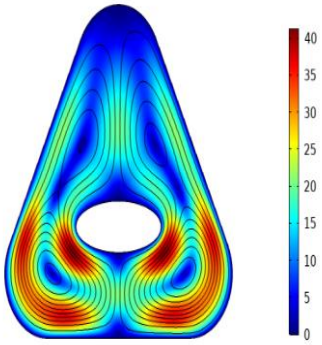	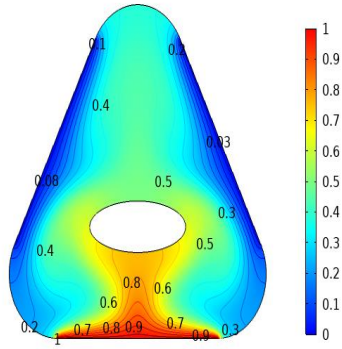	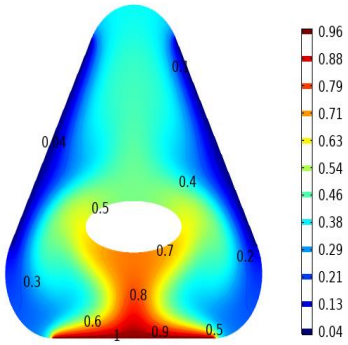
$Ra = 10^6$		
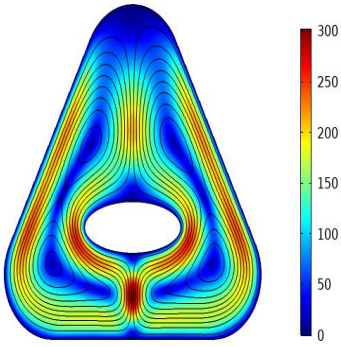	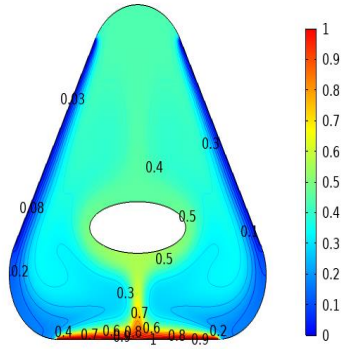	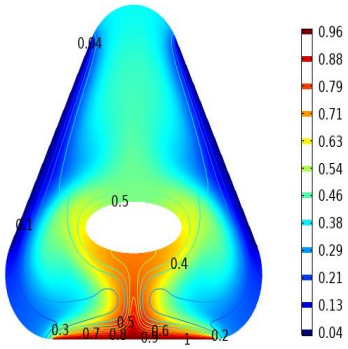

Figure: 5 $(Ha = 20, \gamma = 0, Ra = 10^5,\ Le = 2.5)$

Streamlines	Isotherms	Isoconcentration
$Le = 0.1$		
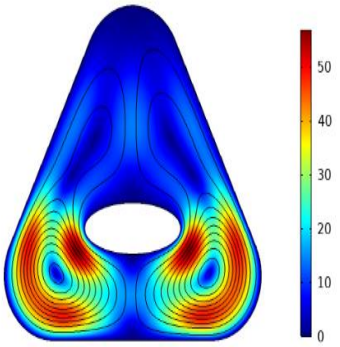	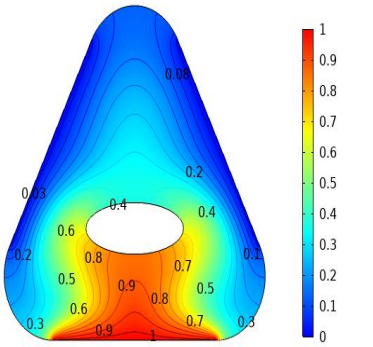	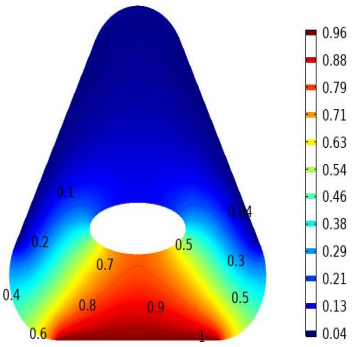
$Le = 1$		
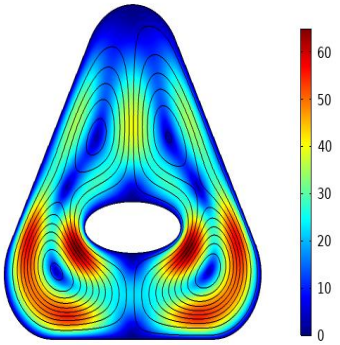	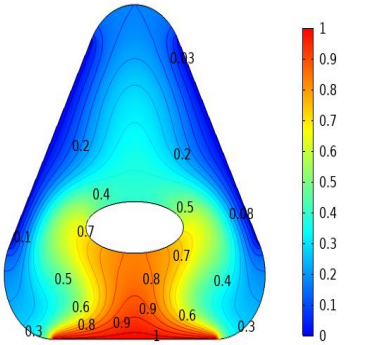	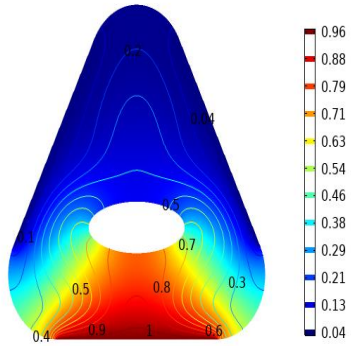
$Le = 10$		
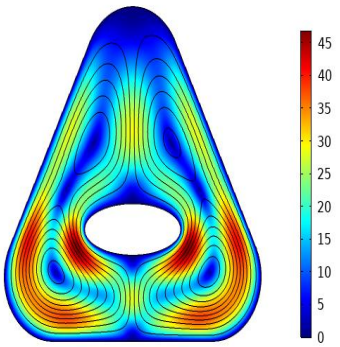	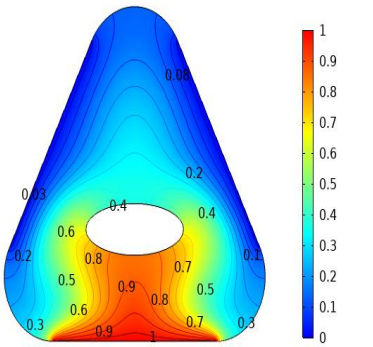	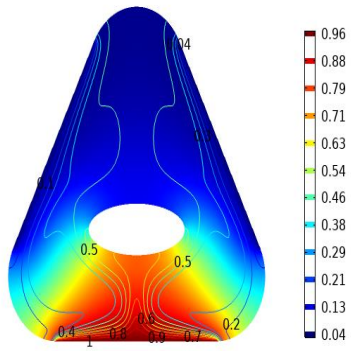

Figure 6: Variation of concentration for various values of *Le*

$Le = 1$ $Le = 2.5$

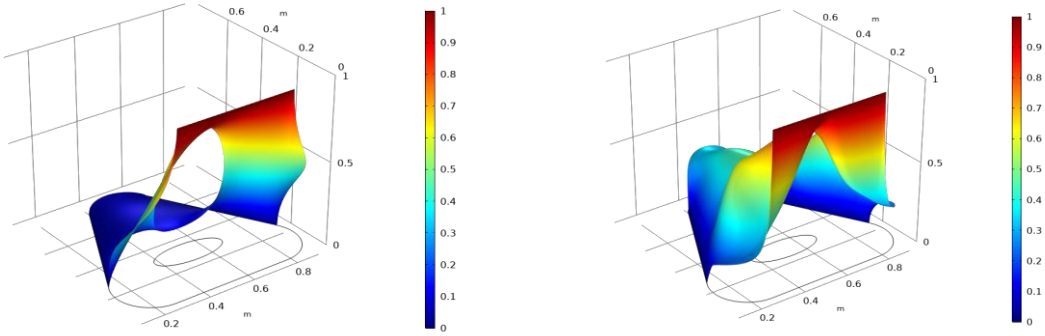

$Le = 7$

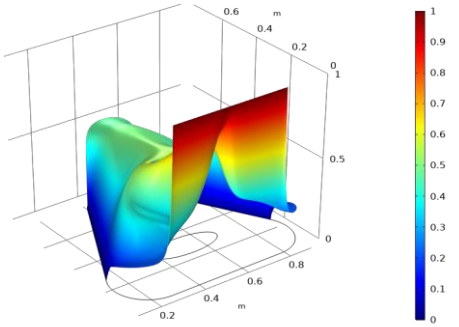

Figure 7: Ha (0,25,50) effects on velocity, temperature and concentration

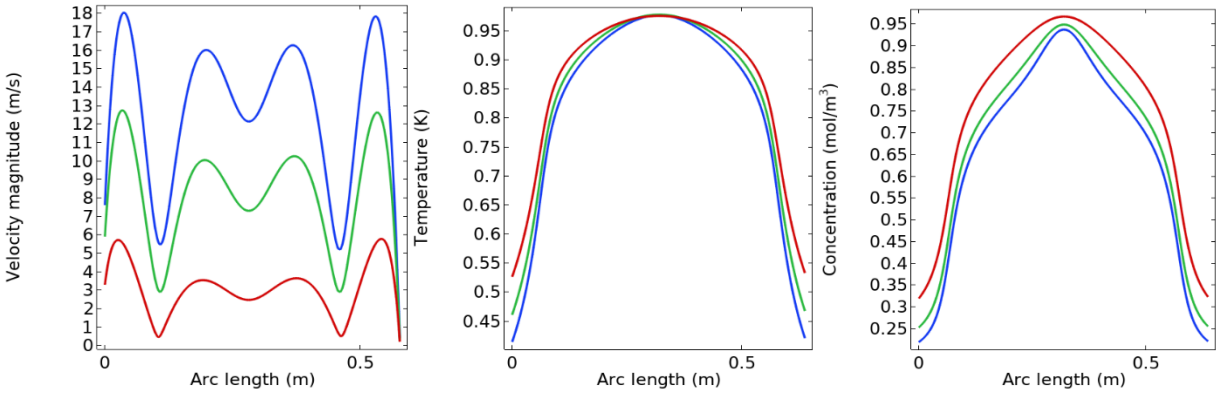

Figure 8: Change in velocity, temperature and concentration for variation in *Le* (5,7,10).

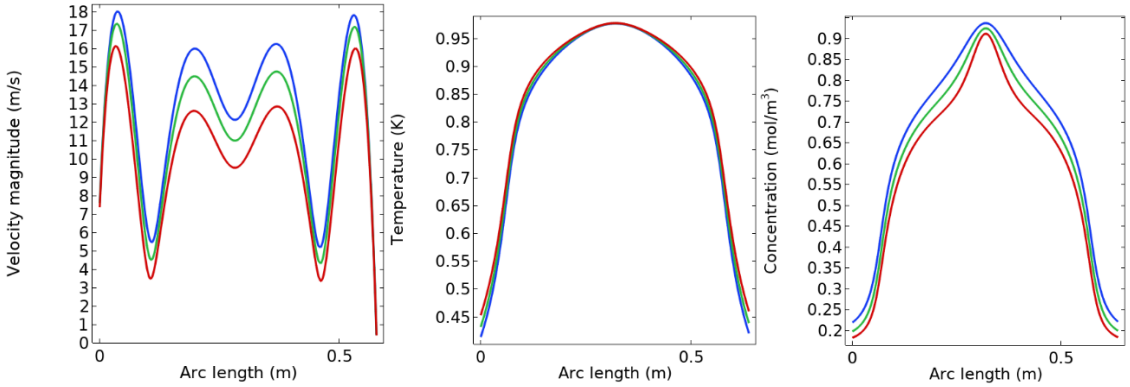

Figure 9: Change in velocity, temperature and concentration for variation in Ra (10^4, 10^5, 10^6).

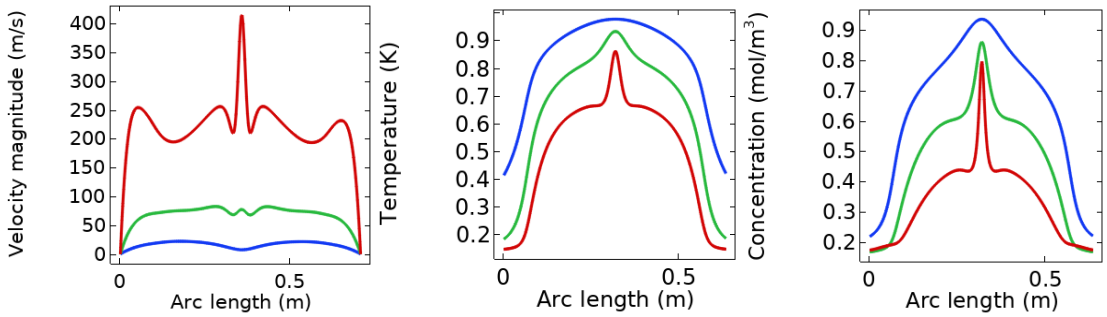

Figure 10: Heat (a) and mass (b) transfer rate versus Hartmann number for variation in *Ra* (10^4, 10^5, 10^6)

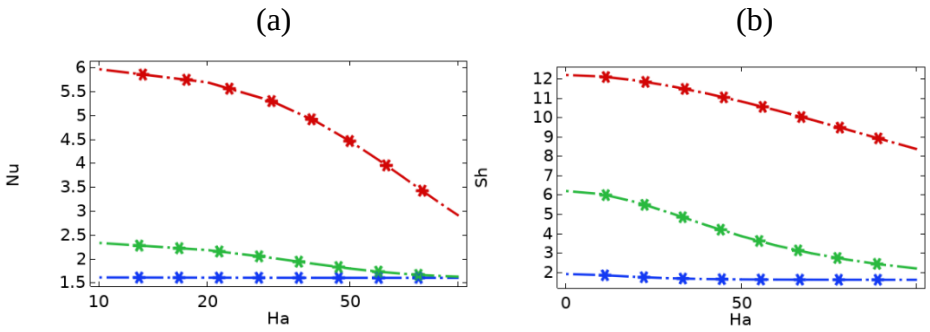

Table.2 Change in heat and mass transfer for variations in Ha. $(\gamma = 0,\ Le = 2.5,\ Pr = 6.8)$

	Heat transfer rate (Nu)			Mass transfer rate (Sh)		
Ha	$Ra = 10^4$	$Ra = 10^5$	$Ra = 10^6$	$Ra = 10^4$	$Ra = 10^5$	$Ra = 10^6$
0	1.62870	3.61027	8.788238	1.792794	5.935344	12.41775
25	1.608398	2.981206	8.293355	1.670083	5.00928	11.96894
50	1.600288	2.176384	7.133760	1.613821	3.540247	10.93293
75	1.598985	1.804213	5.823254	1.602478	2.552625	9.541713
100	1.598809	1.669447	4.684678	1.599763	2.010336	8.049433

Table.3 Change in heat and mass transfer for variations in γ. $(Ha = 0, Le = 2.5,\ Pr = 6.8)$

	Rate of heat transfer			Rate of mass transfer		
Ra	$\gamma = 0^o$	$\gamma = 30^o$	$\gamma = 60^o$	$\gamma = 0^o$	$\gamma = 30^o$	$\gamma = 60^o$
10^4	1.6125	1.6186	1.6179	1.6956	1.7311	1.7273
10^5	3.1711	3.7130	3.8050	5.3041	5.4753	5.6842
10^6	8.4614	8.0395	8.1563	12.118	11.495	11.603

Table.4 Change in heat and mass transfer for variation in Le. $(Ha = 20, \gamma = 30^o, Pr = 6.8)$

	Heat transfer rate (Nu)			Mass transfer rate (Sh)		
Le	$Ra = 10^4$	$Ra = 10^5$	$Ra = 10^6$	$Ra = 10^4$	$Ra = 10^5$	$Ra = 10^6$
0.1	1.6084	2.9367	9.1403	1.5991	1.6188	2.7694
2	1.6147	3.2450	8.6063	1.6686	4.8061	11.309
5	1.6556	3.0111	8.1277	2.5945	7.2863	15.064
7.5	1.6581	2.8849	7.9453	3.2562	8.4941	17.127
10	1.6525	2.7977	7.8295	3.7002	9.3768	18.773

Table 5. Numerical values of Kinetic energy for the variation of Ha, ϕ and γ.

Ra	$\prec Ha = 0 \mid Ha = 25 \mid Ha = 50 \succ$	$\prec \gamma = 0^o \mid \gamma = 30^o \mid \gamma = 60^o \mid \succ$	$\prec Le = 0.1 \mid Le = 2 \mid Le = 5 \succ$
10^4	⟨2.826490|0.953089|0.213979	⟨2.1048|2.4082|2.1807⟩	⟨1.4268|2.0934|4.8608⟩
10^5	⟨300.2700|160.526|50.76216⟩	⟨311.51|453.93|432.92⟩	⟨264.39|319.48|241.34⟩
10^6	⟨6381.706|4344.643|2152.520	⟨7411.3|7032.3|6902.1⟩	⟨19674|7610.2|5948.1⟩